THE JOURNAL OF BIOLOGICAL CHEMISTRY

Vol. 259, No. 16, Issue of August 25, pp. 10004-10011, 1984
Printed in U.S.A.

The Relation between the Internal Phosphorylation Potential and the Proton Motive Force in Mitochondria during ATP Synthesis and Hydrolysis*

(Received for publication, January 13, 1984)

Seiji Ogawa and Tso Ming Lee

From the AT&T Bell Laboratories, Murray Hill, New Jersey 07974

Using ^{31}P NMR and a potassium ion distribution method, the internal phosphorylation potential and the transmembrane electrical potential of intact rat liver mitochondria were measured simultaneously during ATP synthesis and ATP hydrolysis. The ATPase was shown to quickly equilibrate the internal phosphorylation potential with the proton motive force across the mitochondrial membrane. Upon oxygenation of anaerobic mitochondria, there was a very fast increase of ΔpH and a quick uptake of inorganic phosphate prior to the buildup of the internal ATP. Consistent with the chemiosmotic theory, these results showed the presence of proton pumping by the respiratory system from the bulk internal aqueous phase to the bulk external aqueous phase. There was, in the measured energetic parameters, no indication of direct energy coupling or short circuiting protons between the respiratory energy input and the ATP synthesis.

The chemiosmotic theory (1) is a widely accepted description of energy transduction in oxidative and photophosphorylation. In mitochondria, the respiratory system pumps out protons to generate the electrochemical potential gradient for protons (proton motive force) between the two bulk aqueous phases inside and outside mitochondria. The proton-ATPase uses this proton motive force to synthesize ATP by taking up protons from the external medium to the internal medium. In the reverse direction, protons are pumped out by the proton-ATPase during ATP hydrolysis and the proton motive force is generated. Therefore, in the chemiosmotic theory, the proton motive force ($\Delta\mu_H$) and the internal phosphorylation potential (ΔG_p) are expected to be the most important energetic parameters of this energy transduction. Although there is abundant evidence to support the theory, various puzzling observations (2–5) have been reported which seem to challenge the major role of the proton motive force as an energy intermediate in energy transduction. One modified scheme of the theory is the local chemiosmotic model in which some of the protons pumped out by the respiration reaction go to the ATPase directly to synthesize ATP without reaching the bulk aqueous phase. Here, the proton motive force which ATPase sees is different from and higher than that between the two bulk aqueous phases. Although it is difficult to test this model, we have tried to gain more insight into the proton circulation problem by measuring the proton motive force (bulk) and the internal phosphorylation potential simultaneously in intact mitochondria under various energetic conditions.

In the chemiosmotic theory (1) the reaction that the proton-ATPase catalyzes inside mitochondria can be expressed by the following equation (Equation 1).

$$(P_i + ADP)_{int} + nH^+_{ext} \rightleftharpoons (ATP)_{int} + nH^+_{int} \quad (1)$$

The free energy change (ΔG) for the ATP synthesis in the reaction (Equation 1) can be given by

$$\Delta G = \Delta G_p + n\Delta\mu_H \quad (2)$$

where

$$\Delta G_p = \Delta G_p^0 + 2.3(RT/F)\log[ATP]/[P_i]\cdot[ADP]$$

and

$$\Delta\mu_H = \Delta\psi - 2.3(RT/F)/\Delta pH$$

The proton motive force ($\Delta\mu_H$) is the sum of the electrical potential gradient ($\Delta\psi$) and ΔpH across the membrane. The signs of $\Delta\mu_H$ and $\Delta\psi$ are negative and ΔpH is positive. In the previous study (6), we reported the relation between the internal phosphorylation potential ΔG_p and $\Delta\mu_H$ at state 4 or at a high energy state with no net ATP synthesis, using ^{31}P NMR to determine the values of ΔG_p and ΔpH and also measuring the potassium ion distribution to estimate $\Delta\psi$. At state 4, $\Delta G = 0$ in Equation 2 could be assumed and the resultant value of n was between 2 and 3 (2.2–2.4).

In the present study, we have made similar measurements under conditions where net ATP synthesis ($\Delta G \leq 0$) or net ATP hydrolysis ($\Delta G \geq 0$) was present. Although mitochondria under these conditions were not at an energetically steady state, short time resolution measurements (10–15 s) enabled us to follow the time course of the reaction (Equation 1) at low temperature (8 °C). It became possible to compare the changes in $\Delta\mu_H$ and ΔG_p, both of which were directly and simultaneously measured *in situ*. The objective of the present study was to see whether the relationship between ΔG_p and $\Delta\mu_H$ during ATP synthesis differs from this relationship during ATP hydrolysis. These results will be useful in determining the validity of the reaction (Equation 1).

MATERIALS AND METHODS

Rat liver mitochondria were prepared from starved male rats according to the procedure previously referred to (7). Valinomycin was purchased from Boehringer-Mannheim.

Potassium ion selective electrodes were made as described previously (6). The response time (90% of an output change) was about 1 s. The calibration of the electrode used in NMR studies was made inside the NMR magnet under the same condition as in mitochondrial NMR experiments. Values of $\Delta\psi$ in mitochondria in the presence of valinomycin (0.5 nmol/mg of protein) were estimated from the external and the internal K^+ concentrations, the latter of which was deduced from the amounts of total K^+ and the external K^+. The

* The costs of publication of this article were defrayed in part by the payment of page charges. This article must therefore be hereby marked "*advertisement*" in accordance with 18 U.S.C. Section 1734 solely to indicate this fact.

Nernst equation was assumed to hold.

^{31}P NMR spectra were obtained at 145 MHz using a Bruker WM360 spectrometer. Peak positions in NMR spectra were expressed by parts/million from the 85% phosphoric acid peak at 0 ppm as the reference. In actual spectra, the peak of added or endogeneous glycerophosphorylcholine was used as a field marker at −0.494 ppm. A negative sign was given to the lower field side from the phosphoric acid resonance.

The arrangement of a sample container with a K^+ electrode in an NMR probe is depicted in Fig. 1. The sample container with a 20-mm diameter tube in the lower part had a small opening at the bottom where a K^+ electrode was placed. From the top opening of the sample container, a plunger for sample mixing was lowered. The plunger has a plastic disc supported by a glass tube of a reference electrode. The disc had legs so it would not touch the K^+ electrode at the bottom of the container and was used as a paddle for sample mixing. The tip of the reference electrode was set below the disc. A substrate supply line, a H_2O_2 injection line, and a N_2 gas-flushing line were attached to this plunger above the paddle disk. This sample container was placed at the center of the NMR probe coil and the probe had a center hole for the electrode lead wire to pass through. Vertical movements (2 s/cycle) of the plunger were controlled by the computer that was used to take NMR spectra. The injection of H_2O_2 was synchronized with the plunger movement. After these mixing movements of the plunger, it was placed at the top level of the sample solution so as to have the tip of the reference electrode immersed in the sample solution but away from the NMR coil region. The sample volume used was 12 ml and the bottom 8.5 ml of the solution was in the NMR active region. The pick up coil was a double turn Helmholtz coil connected in parallel. The sensitivity of the probe may be seen by a single scan spectrum of 1 mM P_i solution at pH 7.0 in a typical suspension medium used for mitochondria samples (Fig. 1).

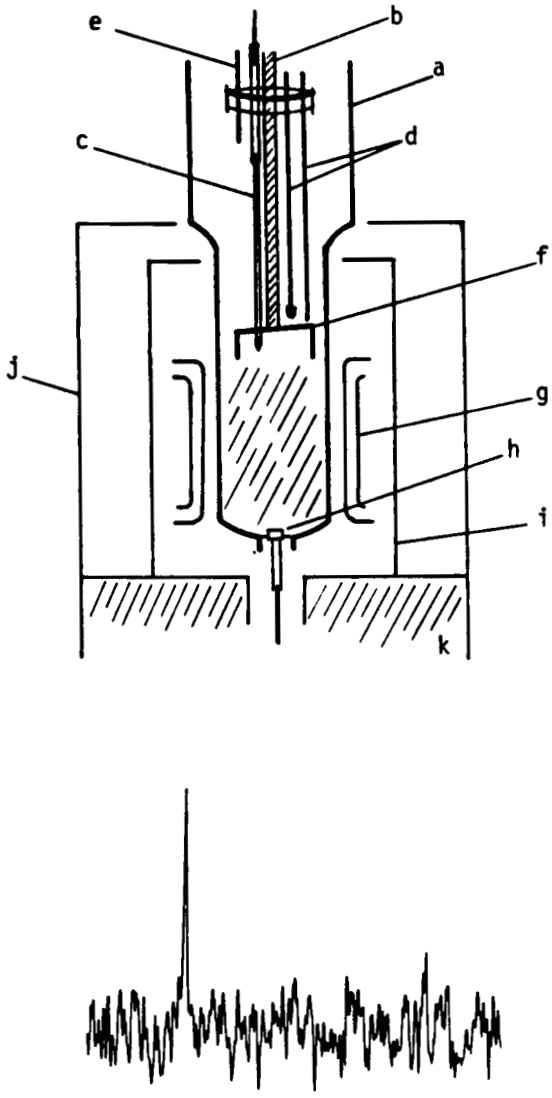

FIG. 1. **The sample container in the NMR probe used in this study (*top*) and ^{31}P NMR peak of 1 mM P_i obtained by a single pulse (*bottom*).** *a*, sample container (Pyrex glass); *b*, supporting rod for the plunger; *c*, reference electrode (Ag/AgCl); *d*, substrate and H_2O_2 supply lines; *e*, gas flow line (N_2 gas); *f*, paddle disc with legs; *g*, RF coil; *h*, K^+ electrode; *i*, thermoshield; *j*, probe cover; *k*, probe coil support. *Bottom*, a P^{31} NMR spectrum of 1 mM P_i in a 10-ml medium which contained 20 mM NaCl and 10 mM glutamate in mannitol solution. One 90° pulse was 30 μs and 20-Hz line broadening was imposed for Fourier transformation. The total width of the spectrum was 6000 Hz.

RESULTS

Oxygen-pulse type experiments[1] were performed in the NMR spectrometer. Anaerobic mitochondria in the NMR sample tube were oxygenated within several seconds by mixing the sample with a controlled amount of H_2O_2 at 8 ± 1 °C. In the presence of valinomycin, the uptake of K^+ into mitochondria was monitored by a K^+ electrode and ^{31}P NMR signals were accumulated at 7.5-s intervals. Within a minute, the external K^+ concentration reached a steady state value and stayed at the value for a while. Then it started to increase, indicating that the sample became anaerobic (Fig. 2*a*). This cycling between the anaerobic and aerobic conditions was repeated several times with the onset of oxygenation as the initiation time. The time courses of these repeated K^+ uptake processes were quite reproducible, provided that the value of the external K^+ concentration at the initiation point was kept constant. The length of the steady state period varied to some extent among these cycles because the amount of oxygen supplied to the sample was not exactly constant. The anaerobic period in a cycle lasted 4.5 min in the experiment shown in Fig. 2*a*. After several cycles, the time course of the K^+ release in anaerobic periods started to show some variation. The ^{31}P NMR spectra taken at various time periods in a cycle were added to those taken in other cycles when the time courses of the K^+ uptake and release in these cycles were superimposable. Those NMR spectra shown in Fig. 3 were obtained by averaging 8 cycles for *a* and *b*, and 3 cycles for *c*–*e*. Their vertical scales were normalized for a constant number of accumulations so as to compare them directly.

Immediately after the oxygenation in the above experiment, the amount of the internal P_i jumped up (Fig. 4*c*) and the increase in ΔpH was very fast (Fig. 4*b*). The ΔpH value stayed constant during the aerobic period. After the start of the anaerobic state, the ΔpH value slowly decreased. The external P_i decreased its intensity after the oxygenation. The decrease was obviously due to the P_i uptake induced by the ΔpH increase and also by the consumption of P_i for the internal phosphorylation (Fig. 3). The intensity of the ATP β-phosphate peak (18.7 ppm) increased from 0 upon the oxygenation and became steady along with the cessation of the uptake of K^+ and decayed when the sample returned to the anaerobic state. Due to the poor signal to noise ratio in NMR spectra, an assumption was made in estimating the amount of ATP by the peak intensity of the ATP β-phosphate resonance. The shape of the peak was assumed to be invariant at various energetic states. This could be justified by the observation that the β-phosphate peak, at early periods after oxygenation,

[1] In usual oxygen pulse experiments (8) the main objective is to measure various initial rates. In the present experiment, the initial stage of the aerobic reaction was masked by a relatively long mixing period. Here we did not aim to measure the initial rates because of the lack of accuracy, but to measure the energetic parameters in as wide a range of their values as possible.

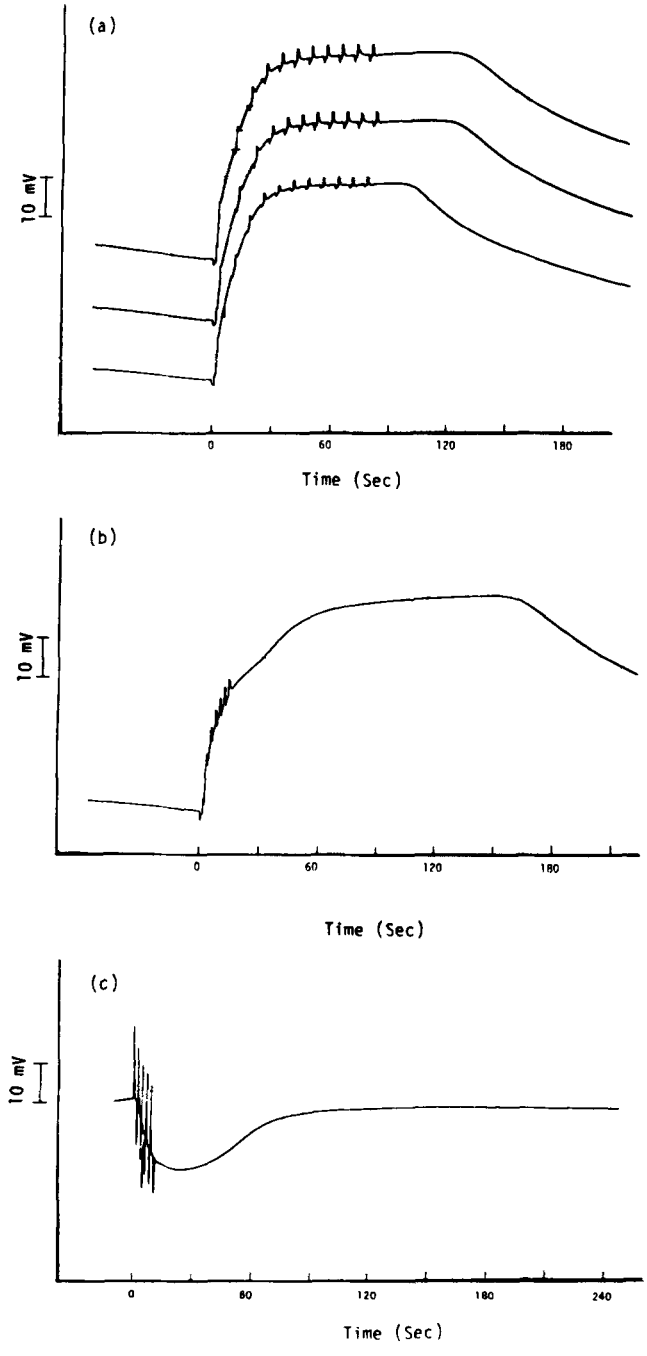

FIG. 2. **Potassium electrode outputs in NMR experiments.** *a*, three cycles of the K^+ electrode output in an oxygen-pulse type experiment are shown. They are aligned at time 0, the start of oxygenation by H_2O_2 injection, and they are shifted vertically for comparison. Spikes in the curves were due to microphonic interferences induced by sample mixing. The time interval for mixing with the injection was 6 s and the first NMR spectrum was collected 10 s after the onset of the oxygenation. Additional mixing of one-pass paddle movement without H_2O_2 injection was made 10 times at 8-s intervals to make the O_2 concentration homogeneous in the sample. The K^+_{ext} concentration at the start of oxygenation was 1.55 mM and it was 0.18 mM at the aerobic steady state. The anaerobic condition lasted 4.5 min before reaching the level of K^+_{ext} where the next cycle was initiated. *b*, similar to *a*, but 1 mM ATP was added. The initial mixing period was 11 s long. There was a delay in the increase of the electrode output at the midway towards state 4. This delay was observed even when the mixing was continued through the period of the output increase. *c*, the time course of the electrode output when ADP (2 mM) was added to a sample at state 4 without the external ATP.

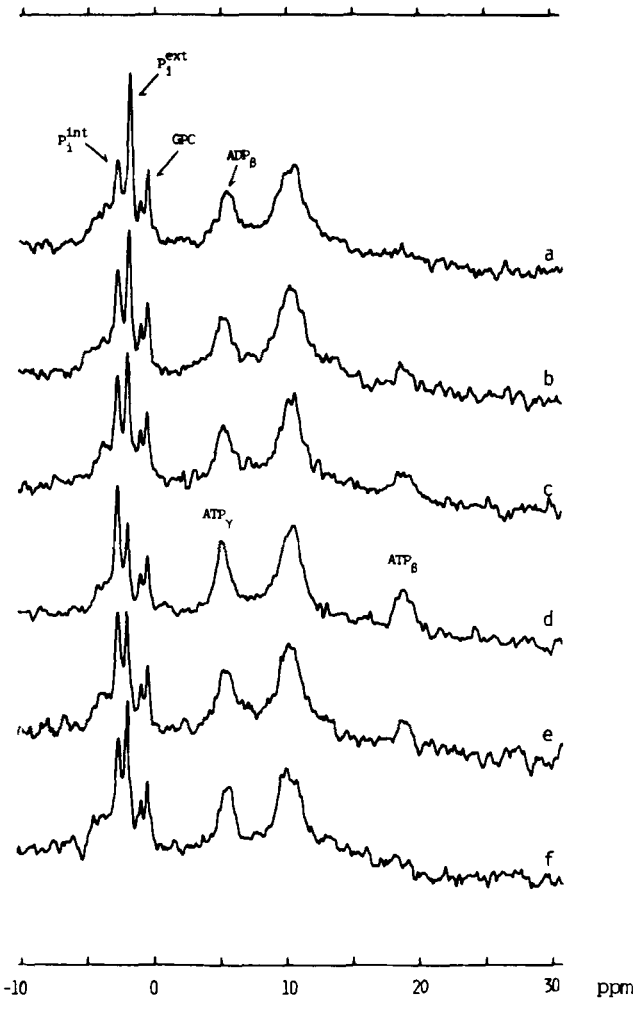

FIG. 3. **^{31}P NMR spectra in an oxygen-pulse type experiment.** Mitochondria (40 mg of protein/ml) were suspended in a mannitol medium which contained 10 mM glutamate, 1 mM P_i, 5 mM EDTA-Na, and 20 mM NaCl. A small amount of glycerophosphorylcholine was added for a reference marker. *a*, 10 s after the start of the oxygenation as shown in Fig. 2*a*. The spectrum was an average of 8 cycles with 16 scans each. *b*, 18 s after the start of a cycle with same averaging as *a*. *c*, 26 s after the start of a cycle with same averaging as *a*. *d*, at the steady state and an average of 32 × 6 scans over 3 cycles. *e*, 30 s in anaerobic state and an average of 32 × 3 scans over 3 cycles. *f*, 80 s in anaerobic state and an average of 32 × 3 scans over 3 cycles. These NMR signals were accumulated with 60° excitation pulses at a 4-s^{-1} repetition rate.

averaged over many spectra, although they are not synchronized in time, was quite similar to the one seen at the steady state. Estimates of the peak intensities were made by the peak height with a constant width, or the area under the peak with a constant shape, and the results were plotted in Fig. 4c. The uncertainties in determining the peak intensities were ±40% at very low ATP levels such as Fig. 3*a* and Fig. 3*e* and ±15% at the steady state.

The initial rate of the K^+ uptake after oxygenation was roughly estimated to be 120 nmol/min/mg of protein. The maximum respiration rate with glutamate was measured to be 10–13 nmol/min/mg of protein in separate experiments with dilute mitochondria samples under very similar conditions. The K^+ uptake appeared to be rapid enough to follow the H^+ pumping at the three sites of the redox reactions in the early stage of the respiration after the start of oxygenation. Therefore, the K^+ ion distribution was assumed to represent

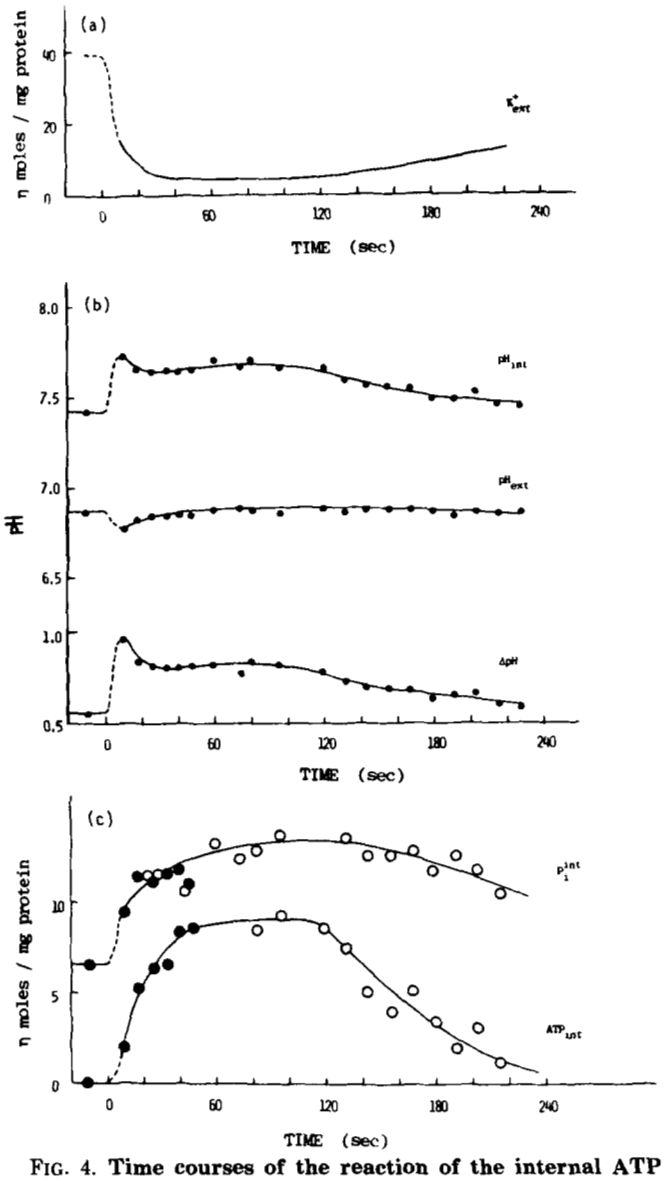

FIG. 4. **Time courses of the reaction of the internal ATP synthesis and hydrolysis.** *a*, the change in the external K^+ in the oxygen-pulse type experiment shown in Figs. 2 and 3. *b*, the internal and external pH and ΔpH. *c*, the change in the internal P_i and the internal ATP in the reaction of *a*. The *filled* and *open circles* were from averages of 8 and 3 cycles, respectively.

the transmembrane electrical potential $\Delta\psi$. Although the development of $\Delta\psi$ with time was observable in this system, without valinomycin the $\Delta\psi$ development would be much faster; the K^+ movement, which provides a large buffering capacity for electrical charge, is no longer available.

It was interesting that during the aerobic period the internal and external pH and, therefore, ΔpH stayed essentially constant except for the early period of oxygenation in spite of the changes in the K^+ distribution and in the levels of the internal ATP and the internal P_i. For an example, 25 s after the oxygenation, the rates of the K^+ uptake, the net ATP synthesis, and the increase of the internal P_i were about 15, 7, and 3 nmol/min/mg of protein, respectively. This K^+ uptake under the constant pH_{int} (or ΔpH) could be explained by the corresponding amount of H^+ pumped out by the respiration which was compensated by the re-acidification of the internal medium due to the P_i uptake and the consumption of P_i inside mitochondria. Two protons for the transport of $H_2PO_4^-$ and its ionization to HPO_4^{2-} at pH 7.7 inside, together with the −1 scalar proton for ATP synthesis, could account for the K^+ uptake.

The amount of the internal ATP plus ADP observable by ^{31}P NMR was estimated from the peak around 5.0 to 5.5 ppm. The position of the peak moved from 5.5 ppm (with no ATP β peak present) to 5.0 ppm (mostly ATP) during the ATP synthesis period and moved back after ATP hydrolysis. The separation of the peaks of the ATP γ- and ADP β-phosphates was relatively small (0.5 ppm or 73 Hz) as compared with the peak width (150 Hz) and, therefore, the apparent peak position in the mixture of ATP and ADP was not useful to estimate the ATP/ADP ratio. However, the shift in the peak position certainly indicated the change in the ratio and the ADP β-phosphate signal intensity should be contributing to the observed peak whenever the presence of the internal ADP was indicated. The content of the internal ADP was estimated from this peak as the sum of the internal ATP and ADP, and the ATP β-phosphate peak at 18.7 ppm as the internal ATP. We assumed that the shapes of the ATP γ- and ADP β-phosphate peaks were invariant. The intensity of the peak was essentially constant except in the cases at early stages after the oxygenation. The difference spectrum from the one at the steady state (high ATP content) showed a slightly lower intensity (15%) in those cases. This lowered intensity was also observed immediately before the oxygenation in these cycles, but the intensity in the ATP hydrolysis period shown in Fig. 4 stayed the same as in the steady state period. Since the sample was kept anaerobic at a fairly low energy state for some time in each cycle before oxygenation, some of the internal ADP was likely converted to AMP by the phosphotransferase activity which was relatively low at this temperature. The spectra 40 s after the oxygenation had essentially no detectable difference in the peak intensity from the steady state spectrum. The ADP β-phosphate peak in an anaerobic state shortly after aerobic incubation without valinomycin had the same intensity as the ATP γ-phosphate peak in aerobic steady state. Therefore, the observable content of the internal ATP plus ADP was estimated from the peak intensity at the aerobic steady state. The amount of ADP at state 4 was small and it was hard to measure. We compared the ADP content measured from the spectrum of an intact mitochondria sample with that measured from the spectrum of the perchlorate extract of the same sample. The spectrum of an intact mitochondria sample (with added $MgCl_2$ at 2 mM and without valinomycin) showed a low level of ADP which was 10% of the ATP and ADP pool and barely detectable. In the presence of Mg^{2+} and without valinomycin, mitochondria seemed to have a slightly higher ΔG_p value. In the extract spectrum, the ADP peak was also very small relative to ATP and the amount was 8% of the ATP and ADP pool which was 10 nmol/mg of protein.

When the spectrum obtained with a 3-s repetition time and 90° excitation pulses in the aerobic steady state was compared with the spectra acquired with a 0.25-s repetition time and 60° pulses, the saturation factor of the ATP γ-phosphate peak was essentially identical to that of the ATP β-phosphate peak. Since the sum of the ATP γ peak and ADP β peak did not depend on the content of ADP, the aerobic reaction of ATP synthesis did not appear to influence the T_1 values of these peaks at the temperature in this study.

The chemical shift (5.5 ppm) of the internal ADP γ-phosphate peak observed in the anaerobic state indicated that the internal ADP was mostly Mg^{2+} bound. If the concentration

TABLE I
Measured energetic parameters of mitochondria

	K^+_{ex}	K^+_{in}	pH_{in}	p_i^{in}	ATP_{in}	$\left(\frac{ATP}{ADP}\right)_{in}$ [a]	ATP_{ex}	$\left(\frac{ATP}{ADP}\right)_{ex}$ [b]	ΔpH	$-\Delta\psi$	$-\Delta\mu_H$	Phos pot.[c]	n_a[d]
	nmol/mg of protein			*nmol/mg of protein*			*nmol/mg of protein*		*mV*	*mV*	*mV*	*mV*	
Experiment 1[e]													
1.1 10 s after oxygenation	15.5	100	7.73	9.5	2.0	0.2			53	119	172	78	2.2
1.2 Steady state	4.6	114	7.65	14	9.2	3.0			45	150	195	136	2.3
1.3 70 s in anaerobic state	9.5	109	7.49	12	3.4	0.4			35	132	167	88	2.4
Experiment 2[f]													
2.1 35 s after oxygenation	4.0	116	7.57	9	4.0	0.9	11	1.8	45	144	189	114	2.2
2.2 Steady state	2.4	118	7.55	12	7.0	4	17	High	42	161	203	145	2.2
2.3 3.5 s in anaerobic state	3.2	117	7.38	13	4.0	0.9	13	3.2	35	152	187	107	2.2
Experiment 3[g]													
3.1 Before ADP addition	3.0	96	7.65	27	6.7	2.4			49	137	186	117	2.3
3.2 30 s after ADP addition	7.6	91.7	7.81	18	4.5	0.9	17	1.1	50	115	165	97	2.4
3.3 Steady state	3.6	95.5	7.86	12	6.0	1.8	33	High	49	133	182	131	2.4

[a] For Mg^{2+}-bound ATP and ADP inside mitochondria.
[b] Mg^{+2}-free ATP and ADP outside mitochondria.
[c] Phosphorylation potential, $(2.3\ RT/F)\log$ ATP/P_i ADP.
[d] The value of ΔG_p^0 (308 mV) at 8 °C was extrapolated from the data reported by Rosing and Slater (9).
[e] 40 mg of protein/ml; experimental conditions were described in Fig. 3. The suspension medium contained 1 mM P_i. For the internal volume, 1.2 μl/mg of protein was used.
[f] 53 mg protein/ml. Similar conditions in Experiment 1 except 1 mM of ATP was added to the sample.
[g] 65 mg protein/ml. The suspension medium contained 3 mM P_i. For the internal volume, 1.6 μl/ml was used.

of the free Mg^{2+} inside mitochondria was below 0.5 mM, the peak should have been shifted upfield by 0.18 ppm from the position of 100% Mg^{2+}-bound ADP[2] and this much of the shift could be detected. A shift of 0.11 ppm would be expected if the free Mg^{2+} concentration was 1 mM. In the present experiment, this was within the uncertainty in determining the peak position of the broad resonance. Since the total Mg^{2+} in mitochondria (25 ng-atoms/mg of protein) is far more than the ATP + ADP pool, the free Mg^{2+} concentration would not have changed drastically from anaerobic state to aerobic state.

Various energetic parameters measured in the experiment described above are listed in Table I. Three similar series of experiments gave very similar results. The correlation between $\Delta\mu_H$ and the internal phosphorylation potential is plotted in Fig. 5. The points with *filled circles* were taken during ATP synthesis and those with *open circles* were taken during ATP hydrolysis. The uncertainty of the measurements, the major part of which was in the determination of the ATP content, are shown by the *bars* at some of these points. The points during periods of both ATP synthesis and hydrolysis lie on the same line. Therefore, within the uncertainty of these measurements, ΔG in Equation 2 for the reaction (Equation 1) was essentially 0 in these experiments. The slope of the line was much closer to 2 than to 3. With the condition of a constant value of ΔG, in this case 0, the stoichiometric number n should be equal to the slope.

$$n = [\partial(\Delta G_p)/\partial(-\Delta\mu_H)]_{\Delta G=0}$$

The slope was 1.8–2.3. However, in the figure all these points are displaced from the lines expected for integer numbers (2 and 3) for the apparent value of n as defined by

$$n_a = \Delta G_p/-\Delta\mu_H$$

Similar to these experiments described above, measurements in the presence of external ATP and ADP were also made. The output of the K^+ electrode (Fig. 2*b*) showed a delay in the growth of $\Delta\psi$ at half way to the steady state. This was likely to be a partial voltage clamp by the external ATP and ADP which influenced the $\Delta\psi$ development through the ATP/ADP exchange transport. Because the amount of ADP was limited in the external medium, this voltage clamp was not complete. The estimated values of various energetic parameters in an experiment of this type were shown in Table I and the relation between ΔG_p and $\Delta\mu_H$ was quite similar to the results shown in Fig. 5. When the proton leakage across the mitochondrial membrane was appreciably increased by adding dinitrophenol, the curve of $\Delta\psi$ development showed slower growth after oxygenation than without dinitrophenol and the value of $-\Delta\psi$ at the steady state was slightly smaller. As expected, the decay of $\Delta\psi$ in the anaerobic state was faster.

It was difficult to generate a state 3 condition (with rapid phosphorylation of external ADP) in a NMR sample under the conditions we used in the present study. Experiments were performed by adding ADP to samples which were at state 4 without external ATP. The change in the K^+ electrode output upon addition of ADP (2 mM) was fast in time as shown in Fig. 2*c*. The period of the lowered $\Delta\psi$ was about 30 s with that amount of added ADP. In this period, the external K^+ concentration did not stay at a steady value but simply passed a maximum value. It was likely due to the rapid change in the ATP/ADP ratio in the external medium by the adenine nucleotide exchange transport. It was noted, however, that even in a dilute mitochondria sample with the same concentration of added ADP, the external K^+ concentration did not become a steady value with state 3 respiration, the rate of which was not constant either. Addition of Mg^{2+} in excess

[2] For these estimates, it was assumed that the shift, if any, from the position of the 100% Mg^{2+} bound ADP was solely due to the degree of Mg^{2+} binding to ADP. The binding constant to ADP in 100 mM KCl, pH 7.5, at 15 °C was measured by NMR to be 0.23 mM. The chemical shifts of the peak with excess Mg^{2+} and without Mg^{2+} were 5.52 and 6.05 ppm, respectively. The binding process was a fast exchange type in contrast to the Mg^{2+} binding to ATP which was slow exchange for the shift of the ATP β-phosphate peak at 145 MHz NMR observation frequency.

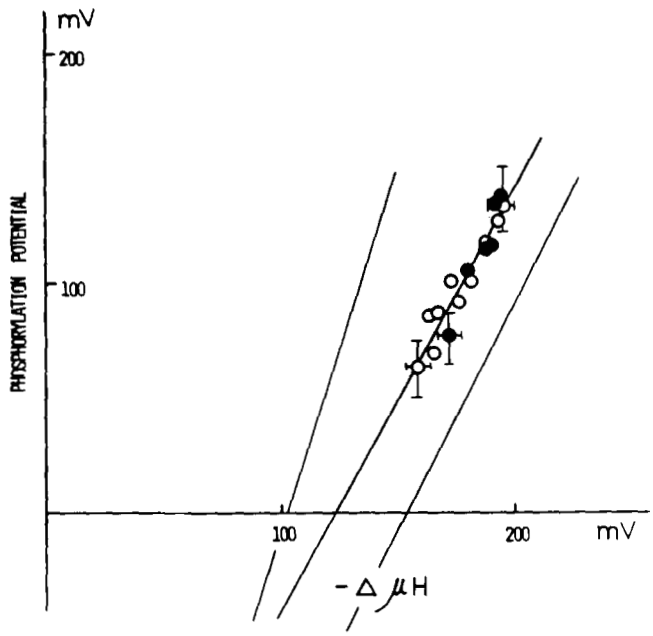

FIG. 5. **The relation of the internal phosphorylation potential to $\Delta\mu_H$.** The results are from the experiment shown in Fig. 4. The *vertical bars* at some points are the uncertainties in ΔG_p due to the ambiguity in the estimates of ATP contents and given at representative points. The *filled circles* are the points during ATP synthesis and the *open circles* are during ATP hydrolysis. Two extra lines are drawn for $n_a = 2$ and 3.

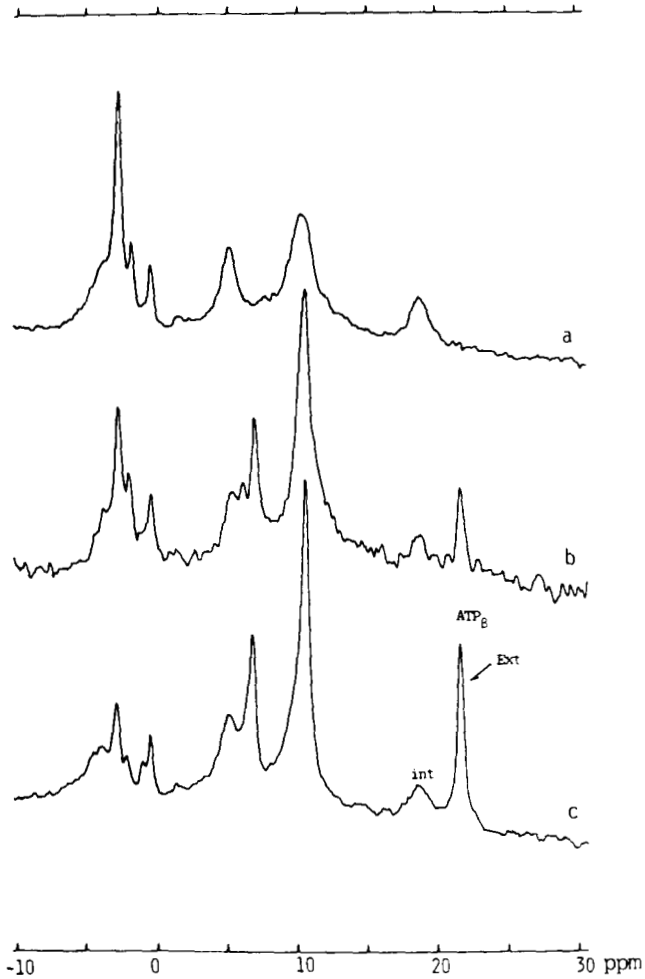

FIG. 6. **^{31}P NMR spectra in a state 3 experiment.** To a mitochondria sample (65 mg of protein/ml) respiring at state 4, 2 mM of ADP was added and the sample was fixed for 10 s. NMR spectra were accumulated separately at 10-s intervals. *a*, before ADP addition. The spectrum was an average of 32 × 12 scans. *b*, 10–40 s after the ADP addition and average of 32 × 3 scans. *c*, at state 4 and average of 32 × 12 scans. These spectra were accumulated with 60° excitation pulses at a 4-s^{-1} repetition rate. The saturation factors (the ratio of the magnetization to the full magnetization without saturation) were 0.40 for the internal P_i, 0.7 for the internal ATP β-phosphate, and 0.27 for the external ATP β-phosphate.

over the amount of EDTA in the medium made the external K^+ concentration quite steady during the state 3 period with a constant respiration rate. In the present NMR experiment, the distinction between the internal and external ATP (Fig. 6) was made by their different chemical shifts due to the presence (internal) and absence (external) of Mg^{2+} bound to the ATP (7). Although some attempts were made to use enzymatic systems to consume ATP in the external medium at a rapid rate, they were not successful in the absence of sufficient amounts of divalent metal ions. The rate of ATP consumption was too low to compete with the phosphorylation by mitochondria.

The time course of the phosphorylation reaction in an NMR sample was measured by accumulating NMR signals every 10 s (Fig. 6). The internal ATP content was estimated from averages of three consecutive spectra in the time sequence (Fig. 6*b*) and the shape of the internal ATP β phosphate peak was assumed invariant. The amount of the phosphorylation which appeared as the increase in the external ATP was estimated by the external ATP β-phosphate peak at 21 ppm.

In the period of 30 s where $\Delta\psi$ was depressed, the internal ATP was 25 to 30% lower than that before the ADP addition. The external ATP appeared quickly after the ADP mixing and the internal ATP did not go down too far (Fig. 7). The ATP/ADP ratio in the external medium in this period changed from 0.4 to 2 as estimated by the external ATP β peak only. The AMP formation by adenylate kinase in the external medium was not significant in the period of this experiment. The internal ATP/ADP ratio (for Mg^{2+}-free compounds) was estimated to be 0.07 using the value of 0.08 for the ratio of the Mg^{2+}-binding constants for ATP and ADP (9). The transmembrane potential $\Delta\psi$ of −115 mV in this period could be compared with the gradients of the ATP/ADP ratio, which changed from −39 to −77 mV. Therefore the ATP-ADP translocase was working in the direction of ATP extrusion with the gradient 40 mV away from equilibrium at the end of the period of the lowered $\Delta\psi$ (10). The internal P_i content changed drastically because of the limited amount of available P_i in the sample. The value of ΔpH did not change appreciably. The energetic parameters are listed in Table I. The mitochondria in the sample contained a substantially larger amount of the internal P_i than those in the other experiments described earlier. The internal volume was likely larger. One estimate made in a sample at similar conditions (3 mM P_i in the suspension medium) was 1.6 μl/mg of protein as compared with the value of 1–1.2 μl/mg of protein in the medium with 1 mM P_i (2). The relation between $\Delta\mu_H$ and the phosphorylation potential was similar to those in Fig. 5.

DISCUSSION

In the oxygen-pulse type experiments, we observed the development of the internal ATP level along with the increase of $\Delta\mu_H$ after oxygenation, then the return of these parameters back to those of the lower energy anaerobic state. These nonsteady state periods were relatively long at the tempera-

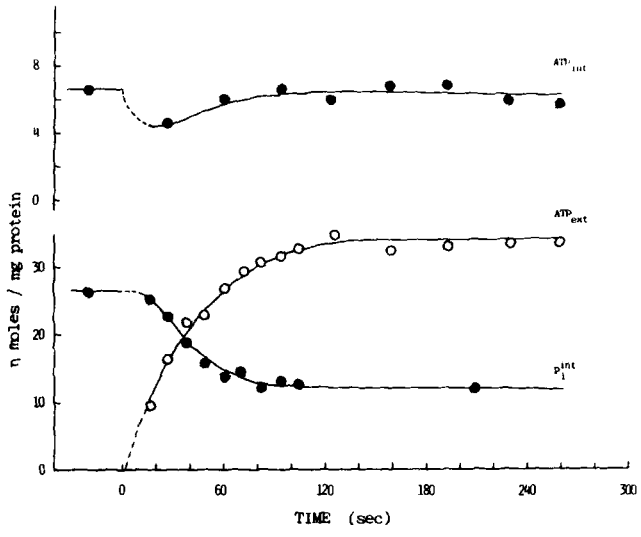

FIG. 7. **Time courses of the phosphorylation reaction in a state 3 experiment.** The plot was obtained from the experiment of Fig. 6. The sample suspension medium contained 3 mM P_i instead of 1 mM P_i as in Fig. 3.

ture used in this study and we could follow the changes by NMR. During these periods, $\Delta G \leq 0$ for ATP synthesis and $\Delta G \geq 0$ for ATP hydrolysis in Equation 2 for the reaction (Equation 1). As shown in Fig. 5, the dependence of the internal phosporylation potential on $\Delta\mu_H$ during ATP synthesis and ATP hydrolysis was essentially the same. Therefore, during the time course of these nonsteady state reactions, $\Delta G \approx 0$ or ATPase was equilibrating the phosphorylation potential with $\Delta\mu_H$. The synthesis reaction proceeded at a faster rate than the hydrolysis reaction by a factor of more than 2. If the ΔG_p increase by the ATPase system was lagging behind the $-\Delta\mu_H$ increase during ATP synthesis ($\Delta G < 0$), the plot of Fig. 5 should have shown hysteresis, having the points during ATP hydrolysis above the points during ATP synthesis. If there were some secondary reaction pathways in addition to the reaction (Equation 1) to make or to consume ATP without the coupling with $\Delta\mu_H$, the points during ATP synthesis in Fig. 5 would have been above the points during ATP hydrolysis. Of course, this statement assumes that the secondary reactions are not reversible as is the reaction (Equation 1). The simplest interpretation of the present results is that the reaction (Equation 1), an expression for the chemiosmotic theory, dominates in the system. There should not be any appreciable contribution to the phosphorylation potential from the secondary reaction pathways, such as direct energy coupling or proton short circuiting to synthesize ATP. The substrate level ATP consumption inside mitochondria is also too slow to compete with the ATPase reaction.

The number of protons required for synthesis of one ATP, n in Equation 2, does not seem to be 3 as judged from the present results. In the plot of Fig. 5, the slope of the line should give the value of n if $\Delta G = 0$ and it was 1.8–2.3. However, the extrapolation to $\Delta\mu_H = 0$ leads to the corresponding ΔG_p^0 which is too small for the standard free energy of ATP synthesis. On the other hand, the apparent value of n, $n_a = \Delta G_p/-\Delta\mu_H$, for those observed points was 2.2–2.4 The noninteger number for n_a could be explained by the local chemiosmotic model or the model of short circuiting protons in the complex of the respiratory system and the ATP-synthesis system. In that model, $-\Delta\mu_H$ is maintained by a transmembrane leak current between the two bulk aqueous phases and the current is supplied by the supramolecular complex which builds the local potential. Therefore, $-\Delta\mu_H$ is an underestimate for the local and true potential to drive the ATP synthesis (5). If this model is applicable, n should be smaller than n_a. For $n = 2$, the underestimate in the proton potential is 20–40 mV in the result shown in Fig. 5. However, in this model one would expect that the relation of ΔG_p to $\Delta\mu_H$ is fairly different between the ATP-synthesis period and the hydrolysis period. During ATP synthesis, the local proton potential to drive the ATPase (or the corresponding $\Delta G_p/n$) must be more than 20–40 mV above the value of $-\Delta\mu_H$. On the other hand, during the ATP-hydrolysis period the bulk proton potential $\Delta\mu_H$ must be supported by not only ΔG_p but also by the K^+ ion distribution in the presence of valinomycin. Actually, the latter had a larger capacity than the ATP system to sustain the leakage current. Therefore, the local proton potential would not be far different from the bulk potential of $-\Delta\mu_H$. In the plot of Fig. 5, the points during the ATP synthesis should be above the points during the ATP hydrolysis period by significant amounts. Therefore, the present results are not consistent with this proton short circuiting model. Furthermore, the ΔpH jump and the P_i uptake, as shown in Fig. 4, preceded the ATP synthesis in time. A significant number of protons appeared in the bulk phases to change the internal pH, which is buffered by at least 10 mM P_i. This proton pumping to the bulk phases in a major way is not consistent with the local proton short circuiting model.

The results from the state 3 type experiments are also in agreement with the above considerations. When the external ATP/ADP ratio changed from far less than 1 to a large number, the apparent value of n (n_a) stayed the same. The time scale of the changes in the relevant energetic parameters in this case were very similar to those in the oxygen-pulse type experiment mentioned above. Therefore, one could expect that the condition of $\Delta G \approx 0$ was also present in the time course of the phosphorylating reaction after the ADP addition. It is interesting to note that the external K^+ ion concentration did not become a steady value in the period of state 3 even in dilute mitochondria samples, just as the respiration rate did not stay constant either. This was in contrast to the constant state 3 respiration with a steady $\Delta\psi$ observed in samples with added Mg^{2+}. From the results of Fig. 7, one could estimate the gradient of the ATP/ADP ratio (Mg^{2+}-free ATP and ADP in both phases) and compare it with $\Delta\psi$. There was a 70–40-mV gap between the gradient and $\Delta\psi$. The activity of the translocator for the adenine nucleotide exchange was not high enough to equilibrate the gradient with $\Delta\psi$. In spite of this energy gap which drove the extrusion of ATP from inside to outside, the internal ATP or ADP level, the $\Delta\psi$, and even the respiration rate varied in the phosphorylation period, apparently sensing the variation of the condition in the external medium.

In the present study, we showed that the internal phosphorylation potential was quickly eqilibrated with $\Delta\mu_H$ by the ATPase and the results are consistent with the chemiosmotic theory except for the noninteger number for n_a.

The present results do not give any supporting evidence for the local chemiosmotic model which was used to explain some of the observations contradictory to the chemiosmotic theory. In the present study, we have focused only on the energetic parameters and not on fluxes such as the respiration rate and the phosphorylation rate. Concerning the regulation of these fluxes, the chemiosmotic theory appears to have some difficulties in explaining various observations (2–4, 11). It seems necessary to know whether the factors that control the fluxes are the energetic parameters or are other factors only indi-

rectly related to the energetics formulated by the chemiosmotic theory.

Acknowledgment—We thank K. A. Ingersoll for his technical assistance in making various devices for sample mixing.

REFERENCES

1. Mitchell, P. (1966) *Biol. Rev. Camb. Philos. Soc.* **41,** 445–502
2. Zoratti, M., Pietrobon, D., and Azzone, G. F. (1982) *Eur. J. Biochem.* **126,** 443–451
3. Padan, E., and Rottenberg, H. (1973) *Eur. J. Biochem.* **40,** 431–437
4. Azzone, G. F., Pozzan, T., and Massari, S. (1978) *Biochim. Biophys. Acta* **501,** 307–316
5. Westerhoff, H. V., Simonetti, L. M., and Van Dam, K. (1980) **200,** 193–202, references therein
6. Ogawa, S., and Lee, T. M. (1982) *Biochemistry* **21,** 4467–4473
7. Ogawa, S., Rottenberg, H., Brown, T. R., Shulman, R. G., Castillo, C. L., and Glynn, P. (1978) *Proc. Natl. Acad. Sci. U. S. A.* **75,** 1796–1800.
8. Lehninger, A. (1978) *Protons and Ions Involved in Fast Dynamic Phenomena*, pp. 435–452, Elsevier, Amsterdam
9. Rosing, J., and Slater, E. C. (1972) *Biochim. Biophys. Acta* **267,** 275–290
10. Krämer, R., and Klingenberg, M. (1980) *Biochemistry* **19,** 556–560.
11. Kell, D. B. (1979) *Biochim. Biophys. Acta* **549,** 55–99